

7-4-2019

## **Experimental Investigation on Thermal Performance of a PV/T-PCM (Photovoltaic/Thermal) System Cooling with a PCM and Nanofluid**

M. M. Sarafraz

Mohammad Reza Safaei

Arturo S. Leon

Iskander Tlili

Tawfeeq Abdullah Alkanhal

*See next page for additional authors*

Follow this and additional works at: [https://digitalcommons.fiu.edu/cee\\_fac](https://digitalcommons.fiu.edu/cee_fac)



Part of the [Engineering Commons](#)

---

This work is brought to you for free and open access by the College of Engineering and Computing at FIU Digital Commons. It has been accepted for inclusion in Department of Civil and Environmental Engineering Faculty Publications by an authorized administrator of FIU Digital Commons. For more information, please contact [dcc@fiu.edu](mailto:dcc@fiu.edu).

---




**Authors**

M. M. Sarafraz, Mohammad Reza Safaei, Arturo S. Leon, Iskander Tlili, Tawfeeq Abdullah Alkanhal, Zhe Tian, Marjan Goodarzi, and M. Arjomandi

---

Article

# Experimental Investigation on Thermal Performance of a PV/T-PCM (Photovoltaic/Thermal) System Cooling with a PCM and Nanofluid

M. M. Sarafraz <sup>1</sup>, Mohammad Reza Safaei <sup>2</sup>, Arturo S. Leon <sup>2</sup>, Iskander Tlili <sup>3</sup>,  
Tawfeeq Abdullah Alkanhal <sup>4</sup>, Zhe Tian <sup>5</sup>, Marjan Goodarzi <sup>6,\*</sup> and M. Arjomandi <sup>1</sup>

<sup>1</sup> School of Mechanical Engineering, University of Adelaide, Adelaide, Australia

<sup>2</sup> Department of Civil and Environmental Engineering, Florida International University, Miami, FL, USA

<sup>3</sup> Department of Mechanical and Industrial Engineering, College of Engineering, Majmaah University, Al-Majmaah 11952, Saudi Arabia

<sup>4</sup> Department of Mechatronics and System Engineering, College of Engineering, Majmaah University, Al-Majmaah 11952, Saudi Arabia

<sup>5</sup> School of Engineering, Ocean University of China, Qingdao 266100, China & Key Laboratory of Fluid Power and Intelligent Electro-Hydraulic Control (Fuzhou University), Fujian Province University, Fuzhou 350108, China

<sup>6</sup> Sustainable Management of Natural Resources and Environment Research Group, Faculty of Environment and Labour Safety, Ton Duc Thang University, Ho Chi Minh City, Vietnam

\* Correspondence: marjan.goodarzi@tdtu.edu.vn; Tel.: (+1)-502-432-0339

Received: 13 June 2019; Accepted: 2 July 2019; Published: 4 July 2019



**Abstract:** In the present work, an experimental investigation is performed to assess the thermal and electrical performance of a photovoltaic solar panel cooling with multi-walled carbon nanotube–water/ethylene glycol (50:50) nano-suspension (MWCNT/WEG50). The prepared nanofluid was stabilized using an ultrasonic homogenizer together with the addition of 0.1vol% of nonylphenol ethoxylates at pH = 8.9. To reduce the heat loss and to improve the heat transfer rate between the coolant and the panel, a cooling jacket was designed and attached to the solar panel. It was also filled with multi-walled carbon nanotube–paraffin phase change material (PCM) and the cooling pipes were passed through the PCM. The MWCNT/WEG50 nanofluid was introduced into the pipes, while the nano-PCM was in the cooling jacket. The electrical and thermal power of the system and equivalent electrical–thermal power of the system was assessed at various local times and at different mass fractions of MWCNTs. Results showed that with an increase in the mass concentration of the coolant, the electricity and power production were promoted, while with an increase in the mass concentration of the nanofluid, the pumping power was augmented resulting in the decrease in the thermal–electrical equivalent power. It was identified that a MWCNT/WEG50 nano-suspension at 0.2wt% can represent the highest thermal and electrical performance of 292.1 W/m<sup>2</sup>. It was also identified that at 0.2wt%, ~45% of the electricity and 44% of the thermal power can be produced with a photovoltaic (PV) panel between 1:30 pm to 3:30 pm.

**Keywords:** photovoltaic/thermal system; multiwalled carbon nanotube; equivalent electrical–thermal power; phase change material; paraffin

## 1. Introduction

Management of the chain of energy supply and preventing environmental pollution has led to a growing interest in renewable technology as a potential alternative to fossil fuel. A census has been reached that conventional fuels can potentially have significant economic, environmental, and social

effects. It causes enormous annual costs originating from the pollutants released during the extracting, processing, and fossil fuel transferring, which affect environmental and human health [1]. Solar energy is by far one of the potential options for the production of thermal and electrical power which can supply the required energy demand on earth [2]. Solar energy can be tailored to a variety of applications including (but not limited to) industrial processes, domestic and agricultural use, space programs, and smart houses and residential buildings [3–5]. Production of electricity via solar panels is one viable option to supply the electricity demand. PV systems are applicable for agriculture and common uses, in the form of independent power station or coupled to a global network along with fixed or movable configurations, whether small units with low power such as electricity energy for a simple calculator or giant power station systems for domestic use [6–8]. Despite the fact that photovoltaic (PV) panels are a promising option for future electricity production, the increase in the temperature of the panel causes a reduction in the efficiency of the electricity. Chow et al. [9] reported that the performance of a PV system can potentially decrease up to 5% by a 10 °C increase in the temperature of the panel. Thus, cooling the PV systems is a key challenge, which requires further research and development.

To efficiently cool a solar PV, one potential option is to attach a solar collector to the backside of a solar PV [10–12]. This can remove the heat produced by the solar panel referred to as “photovoltaic/thermal system” [13]. By doing this, the system operates at a lower temperature, and therefore higher electrical performance is achieved [14,15].

Since the application of the nanofluid in various thermal engineering systems was demonstrated, special attention has been paid to the thermo–physical characteristics of the nanofluids [16–18]. It has been reported that by using a nanofluid with high concentration at high velocity, a solar thermal collector can operate with 76% higher efficiency than it does with conventional coolants [19]. For example, Yazdanifard et al. [20] conducted a series of experiments to investigate the performance of a plate PV/thermal (PV/T) systems working with nanofluids in the laminar and turbulent flow regime. They tested aqueous nanofluids of Al<sub>2</sub>O<sub>3</sub> and TiO<sub>2</sub> at volume fractions of 0% to 4% and diameter ranged between 21 nm and 100 nm. They observed that nanofluid promotes the thermal performance of the PV/T panel when compared to pure water or ethylene glycol. It was also identified that Al<sub>2</sub>O<sub>3</sub> nanoparticles represent better thermal characteristics in comparison with TiO<sub>2</sub>. The performance of a PV/T system cooling with Al<sub>2</sub>O<sub>3</sub>/water, CuO/water, and TiO<sub>2</sub>/water as nanofluids was analyzed by Sahota et al. [21]. They found that the nanofluid can improve the efficiency of the PV/T system and reported that CuO/water has the highest thermal efficiency (80.18%).

Recently, the potential application of phase change materials has been investigated by several researchers with the view to further improve the thermal performance of a PV/T system, while decreasing the heat loss and exergy destruction from the system. In most of the studies, the thermal characteristics of the phase change material are improved by adding nanoparticles to the bulk of the phase change material (PCM) [22,23], which enhances the thermal conductivity and thermal storage capability of PCM [24]. For example, Kazanci et al. [25] examined the performance of a PCM used in a PV/T system. They found that by utilizing the PCM, the electricity production of the PV panel can be improved by 15.5%. Al-Waeli et al. [26] utilized SiC nanoparticles with mass fractions 0% to 4% in paraffin-PCM to analyze the thermal and electrical performance of a hybrid PV/T panel. They reported that the heat dissipation from the PV/T panel was more uniform when PCM was used in the system. The presence of PCM further improved the efficiency of the system from 7.1% to 13.7% in comparison with the conventional PV systems. The effect of ZnO/water nanofluid and paraffin wax PCM was experimentally studied by Sardarabadi et al. [27] in a PV/T system. They used nanofluids with concentrations of 0wt%, 0.1wt%, 0.2wt%, and 0.4 wt% and noticed that the electrical efficiency is enhanced by 13%. The efficiency of PV/T system with nanofluid was 5% larger than that recorded for PV/T cooled with pure water. Also, a PCM further enhanced the efficiency of the PV panel by 9%. In another study, Al-Waeli et al. [28] experimentally investigated the performance of a hybrid PV/T system and numerically evaluated the economic performance of the system. They utilized 0wt% to 4 wt% of SiC/water nanofluid and paraffin wax as a PCM material. Results indicated electrical

performance and thermal efficiency enhance by 13.7% and 72%, respectively. There is extensive research conducted on the performance analysis of PV/T systems, which has been summarized in Table 1.

**Table 1.** Several pieces of research about photovoltaic/thermal (PV/T) systems with nanofluids and/or phase change materials (PCMs).

Author (s)	Type of Study	Nanofluid and/or PCM Materials	Concentration of Nanofluid	Achievements
Hosseinzadeh et al. [29]	Numerical	ZnO/water Paraffin wax	0.2wt%	Improvement of thermal energy: 79.36% Electrical efficiency: 13.36%
Al-Waeli et al. [30]	Experimental and mathematical	SiC/water	3wt%	Electrical efficiency (experimental): 13.7% Thermal efficiency (experimental): 72% Electrical efficiency (mathematical): 13.2% Thermal efficiency (mathematical): 71.3%
		Nano-PCM	0.1%, 0.5%, 1%, 2%, and 3%	
Hassan et al. [31]	Experimental	SiO <sub>2</sub> , SiC, TiO <sub>2</sub> in water	1wt%	SiC had the highest efficiency; Electrical efficiency: 12.75% Thermal efficiency: 85% Overall efficiency: 97.75%
Al-Shamani et al. [32]	Experimental	SiO <sub>2</sub> , SiC, TiO <sub>2</sub> in water	0wt%–2wt%	SiC had highest efficiency; Electrical efficiency: 13.52% Thermal efficiency: 81.73%
Imtiaz Hussain et al. [33]	Numerical	CuO, Al <sub>2</sub> O <sub>3</sub> , SiO <sub>2</sub> in water	0vol%–0.75vol%	SiC had the highest efficiency; Total equivalent efficiency: 90.3%
Al-Waeli et al. [34]	Experimental	CuO, Al <sub>2</sub> O <sub>3</sub> , SiC in water	0.5vol%, 1vol%, 2vol%, 3vol%, and 4vol%	SiC had the highest efficiency; Total equivalent efficiency: 16.8% Thermal efficiency: 50%
Al-Waeli et al. [35]	Numerical	CuO, Al <sub>2</sub> O <sub>3</sub> , SiC in water, glycerin, and ethylene glycol	4wt%	SiC had the highest convective heat transfer and glycerin had maximum pressure drop. SiC nanoparticles had 1.21% and 2.15% higher Nusselt number compared to CuO and Al <sub>2</sub> O <sub>3</sub> nanoparticles, respectively.
Aberoumand et al. [36]	Experimental	Ag/water	2wt% and 4wt%	Power output enhancement: 35% Exergy efficiency: 50%
Lari et al. [37]	Numerical	Ag/water Paraffin wax	0.5vol% Added surfactant: 1wt%	Electrical efficiency: 11.7% Thermal efficiency: 11.7%
Al-Waeli et al. [38]	Experimental and ANN modeling	SiC/water SiC nano-paraffin wax	Nanofluid: 0–4 wt%	Electrical efficiency enhanced from 8.07% to 13.32 than to the simple PV.
Abdallah et al. [39]	Experimental	MWCNT/water	0–0.3 vol%	Overall efficiency: 83.26%
Al-Waeli et al. [40]	ANN modeling	SiC/water SiC nano-paraffin wax	0–4% both nanofluid and nano-PCM	Thermal efficiency: 72%
Salem et al. [41]	Experimental	water and/or Al <sub>2</sub> O <sub>3</sub> /PCM mixture	0–1 wt%	Highest efficiency was achieved for pure PCM/water
Fayaz et al. [42]	Experimental and numerical	Paraffin wax		PVT electrical efficiency (experimental): 12.28% PVT electrical efficiency (Numerical): 12.4% PVT-PCM electrical efficiency (experimental): 12.59% PVT-PCM electrical efficiency (numerical): 12.75% PVT electrical performance (experimental): 9.2% PVT electrical performance (Numerical): 10.13% PVT-PCM electrical efficiency (experimental): 12.75% PVT-PCM electrical efficiency (numerical): 12.91%
Fayaz et al. [43]	Experimental and numerical	Paraffin wax		Electrical efficiency of PV/T-PCM (experimental): 13.87% Electrical efficiency of PV/T-PCM (numerical): 13.98% Electrical performance of PV/T-PCM (experimental): 7.6% and electrical efficiency of PV/T-PCM (numerical): 7.2%

Facing the above literature, it can be concluded that the efficiency of PV/T systems can potentially be improved by using metallic nanoparticles together with a PCM at the backside of the panel. In the present work, the potential application of multi-walled carbon nanotube dispersed in water/ethylene glycol 50:50 (by volume) as a coolant in a PV/T system is experimentally investigated. To further improve the thermal performance of the panel and to increase the thermal absorption from the backside, carbon nanotube–paraffin nano-suspension was used as a PCM. The influence of the mass concentration of the nanofluid, flow rate of cooling loop and time of the day on the thermal and electrical efficiency of the PV panel was experimentally investigated and discussed. The equivalent thermal–electrical performance of the PV panel was also investigated as a performance criterion.

## 2. Experimental

### 2.1. Test Rig

Figure 1A represents the schematic diagram of the test rig used in the present research. In order to utilize the same solar irradiance profile, five similar test rigs were used to conduct the experiments in a similar condition. Each test rig included a nanofluid and/or water tank containing the heat transfer fluid (HTF). A 12-volt gear pump was used to circulate the HTF within the cooling loop. A bypass loop and a valve were employed to control the flow rate of the coolant within the PV panel. The flow rate of the fluid was measured with an ultrasonic flow meter (it is not shown in Figure 1) connected to a data logger. The outlet from the PV panel was cooled in a shell and tube heat exchanger constantly fed with water at 25 °C. The inlet and outlet temperatures of the HTF were recorded and logged with two Resistance temperature detectors (RTD) thermo-meters. Two digital multi-meters were employed to constantly record the current and the voltage of the photovoltaic panel. The produced electricity was stored in a battery storage, while the hot water produced with the heat exchanger was stored in a heavily insulated water tank. Figure 1B shows the schematic representation of the cooling jacket which not only is a PCM container, but also provides conditions to contact the PCM with the metallic body at the backside of the PV. The piping arrangement was parallel, and the flow direction was upward from the bottom of the PV towards the upper side. By doing that, not only the residence time of fluid was increased but also the heat loss from the PV panel could potentially be decreased and the thermal energy produced with the PV panel could completely be absorbed by the PCM. To improve the thermal energy absorption, multi-walled carbon nanotubes (MWCNTs) were also dispersed in paraffin to further increase the thermal conductivity of the PCM, which in turn improved the thermal diffusivity coefficient of the PCM. Notably, the presence of MWCNTs can slightly decrease the heat capacity (~3%), however, the anomalous enhancement in the thermal conductivity of the PCM can compensate for this reduction.

To conduct the experiments, first, the system was allowed to operate for an hour to de-aerate the pipes, joints and the pump hose. Then, the measurement devices were turned on to continuously measure the temperature and flow rate. The experiments were conducted under standards defined by the American Society of Heating, Refrigerating and Air-Conditioning Engineers (ASHRAE) 96 (amended version in 1980). To measure the solar irradiance, pyrano-meter HOB0 RXW LIB900 (accuracy:  $\pm 10$  W/m<sup>2</sup>) was employed (range of measurement: 0–1280 W/m<sup>2</sup> within the spectrum of 300–1100 nm) located above the PV panels. Four wireless sensors were connected to the pyrano-meter to increase the accuracy of the data readings. The dimension of the sensor was 4.1 cm (length)  $\times$  3.2 cm (diameter). The experiments were conducted in a place with coordinates of 27.1832° N and 56.2666° E.

Notably, the thickness of the copper-made cooling jacket was 3 cm and the diameter of the cooling pipes was 2.54 cm. About 3.4 kg of paraffin was also used within the system to fill the gaps between the cooling pipes and the surface of the PV panel. Also, insulation was used to ensure that the heat loss from PCM to the environment was negligible. The cooling jacket was made from copper to minimize the thermal resistance between the PV panel and the PCM.

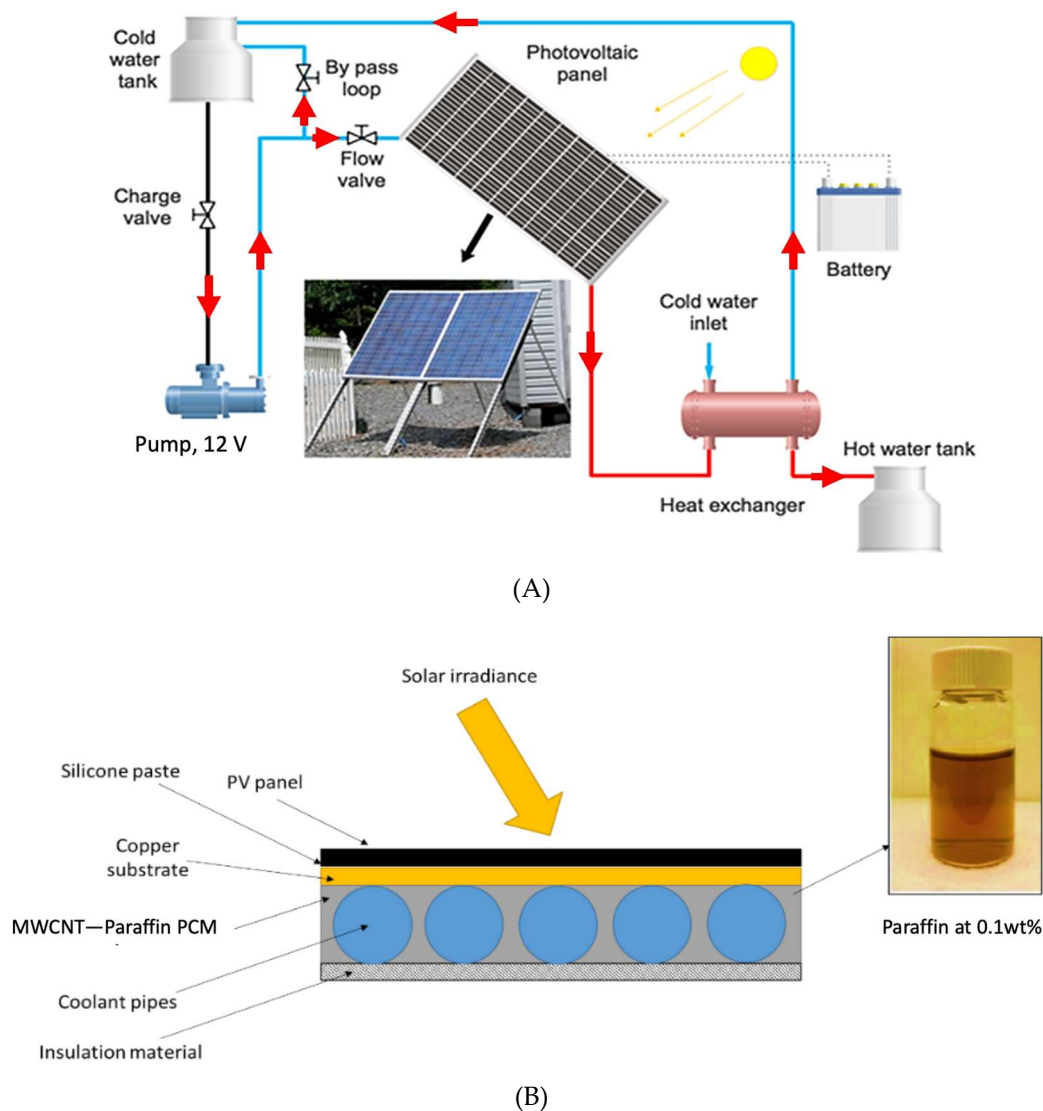


**Figure 1.** Schematic diagram of the test rig and the PCM container used in the present work. (A) Schematic diagram of the experimental setup, (B) cooling jacket of the PV panel and the PCM container.

## 2.2. Preparation and Characterization of the Nanofluid

In the present work, the electrical and thermal energy production of the PV panel were quantified. Hence, the thermal characteristics of the HTF played the major role in the efficiency of the system. To prepare the nanofluid, the following procedure was applied:

- 1- The desired mass of multiwalled carbon nanotube was dispersed in water/ethylene glycol 50:50 (by volume). To quantify the mass of the nanoparticles, a balancer with an accuracy of 0.0001 g was employed.
- 2- An ultrasonic homogenizer was employed to uniformly disperse the MWCNTs within water/ethylene glycol (50:50) nano-suspension (WEG 50). The frequency, timer, and power throughput of the device were set to 20 kHz, 10 min and 30 Watt to ensure that the base fluid would not evaporate and the structure of the carbon nanotube would not be affected by ultrasonic waves.
- 3- Nonylphenol ethoxylates at 0.1vol% was used to further increase the stability of the nanofluid by decreasing the surface tension and the attractive forces within the bulk of the nanofluid.

Characterization tests were conducted to evaluate the dispersion of the MWCNTs in WEG 50 and to ensure that the structure of MWCNT was in accordance with the standard pattern obtained for MWCNT with purity >99.99%. Notably, the impurity involved in the structure of CNTs can strongly affect the thermal conductivity and other heat transfer characteristics of the nano-suspension. Hence, transmission electron microscopy and X-ray diffraction tests were utilized to ensure about the uniform dispersion and the structure of the samples. As can be seen in Figure 2A, the multi-walled carbon nanotubes have been dispersed within the sample uniformly and clustering and axial agglomeration of the MWCNTs cannot be seen within the sample. Also, Figure 2B shows the X-ray diffraction (XRD) pattern obtained for the MWCNT samples. As can be seen, the identified peaks are in accordance with the peak numbers reported for the MWCNT and there is no impurity within the structure of MWCNTs. Also, time-settlement experiments were conducted to obtain the chemical conditions in which the MWCNT/WEG 50 was stable. To improve the stability of the nanofluid, pH setting using HCl + NaOH buffer solution (0.1 mM) was utilized resulting in the promotion of the stability of the nanofluids up to three weeks (at 0.3wt%). The longest stability for nanofluid at 0.3wt% was obtained at pH = 8.9 and after 10 min of sonication at 20 kHz.

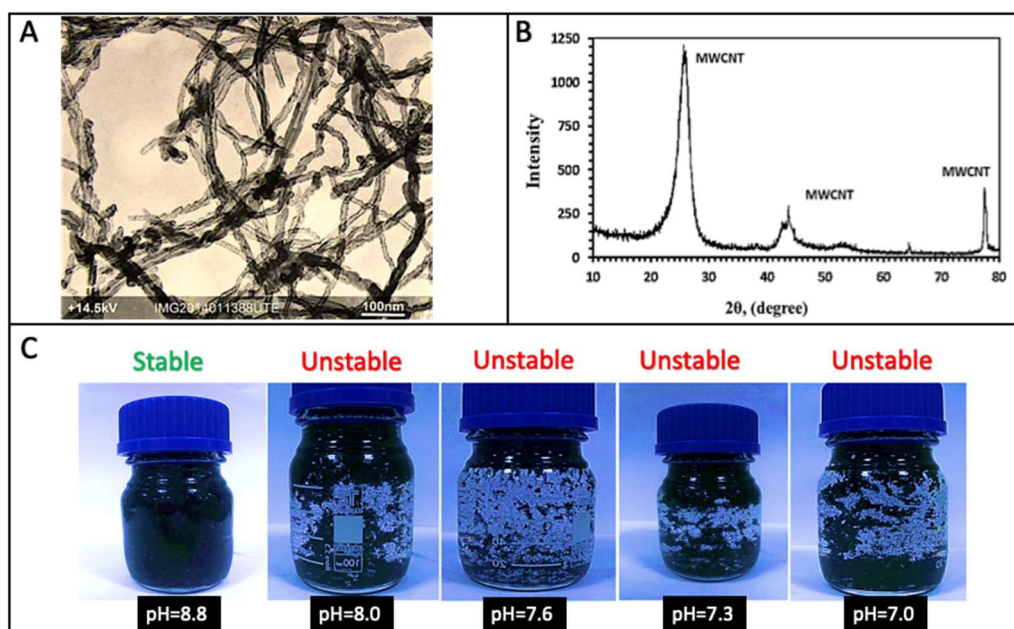


**Figure 2.** Characterization of the multi-walled carbon nanotube–water/ethylene glycol (50:50) nano-suspension (MWCNT/WEG50) nanofluid. (A) TEM image taken from the nanofluid at 0.1wt%, (B) X-ray diffraction (XRD) pattern obtained from solid MWCNTs, (C) effect of pH setting on the stability of the nanofluid three weeks after the preparation taken by blue fluorescence non-flicker light.

Since thermo–physical properties of the nanofluid play a major role in the thermal performance of the system, the density, thermal conductivity, and heat capacity of the nanofluids were measured experimentally. Likewise, the thermal conductivity of the PCM was also measured to ensure that the presence of MWCNTs could improve the thermal feature of the PCM. To measure the heat capacity and thermal conductivity of the nanofluids Decagon KD2 pro was used (accuracy:  $\pm 1\%$  of reading value) and to measure the density, the density meter DM45 manufactured by Anton-Paar (accuracy:  $\pm 1\%$  of reading value) utilized. Figure 3 presents the variation of the thermo–physical properties of the nanofluid including thermal conductivity, density, and heat capacity with the mass fraction of MWCNTs dispersed in WEG 50. In addition, the thermal conductivity of paraffin was assessed at various mass fractions of MWCNTs. Results were merged into one figure represented as Figure 3. Here, “M” is a thermo–physical property and “ $M_0$ ” is the same thermo-physical property for WEG 50 and paraffin, respectively. As can be seen, for thermal conductivity, with an increase in the mass



fraction of the nanofluid, the thermal conductivity of the nanofluid increased. The largest thermal conductivity enhancement was ~23% belonging to nanofluid at 0.3wt%, in which the Brownian motion of MWCNTs is maximized. Also, it is expected that the thermal conductivity of the nanofluid is further enhanced due to the thermo-phoresis effect, which improves the migration of the nanoparticles due to the temperature difference within the bulk of the nanofluid. Also, density of the nanofluid increases with an increase in the mass fraction of the MWCNTs. The largest augmentation for the density was ~5% at 0.3wt%. The heat capacity of the nanofluid was also decreased with an increase in the mass fraction of MWCNT. This is because the heat capacity of WEG 50 is relatively larger than MWCNT. Hence, with an increase in mass fraction of MWCNT, the contribution of WEG 50 in heat capacity of mixture decreases resulting in a small decrease in the heat capacity of the nano-suspension. The maximum reduction was ~3% recorded at 0.3wt%. For MWCNT–paraffin, it was found that with an increase in the mass fraction of MWCNTs, the thermal conductivity of paraffin increased by ~8%, 13.4%, and 19% for 0.1wt%, 0.2wt%, and 0.3wt%, respectively. Hence, to maximize the thermal conductivity of PCM, nanoparticles were dispersed in PCM at 0.3wt%.

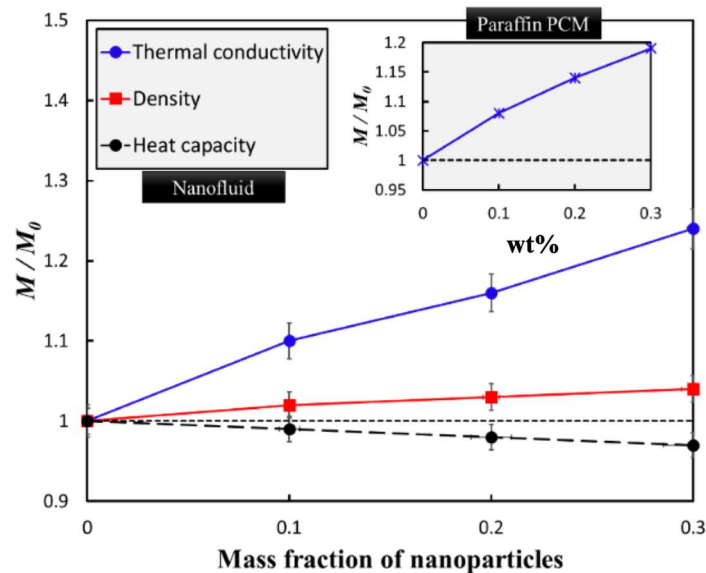


**Figure 3.** Variation of the thermo–physical properties of the nanofluid and PCM with mass fraction of the nanoparticles.

### 2.3. Data Reduction and Uncertainty Analysis

To quantify the thermal energy produced with the PV panel, Equation (1) was employed:

$$E_{th} = \dot{m}C_p(T_O - T_{in}), \quad (1)$$

where,  $E_{th}$  is the thermal energy produced with PV panel,  $\dot{m}$  is the mass flow rate of the working fluid,  $C_p$  is the heat capacity of the working fluid,  $T$  is the temperature and  $O$  and  $in$  stand for outlet and inlet ports of the PV panel. To calculate the electrical power produced with the PV panel, the following equation was utilized:

$$E_{el.} = V_{OC}I_{SC}FF_{eff.}, \quad (2)$$

where,  $E_{el.}$  is the electrical power produced with PV panel,  $V_{OC}$  and  $I_{SC}$  are voltage and current of the open circuit and short circuit measured with a multi-meter.  $FF_{eff.}$  is the filled factor considering the pumping power of the nanofluid, which strongly depends on the  $V_{OC}$  and is inversely proportional to the temperature of the PV panel and also changes with mass concentration of the nanoparticles (due to the change in  $E_{pump}$ ), which can be calculated with the following equation:

$$FF_{eff.} = \frac{\text{Maximum electrical power} - E_{pump}}{V_{OC}I_{SC}} \tag{3}$$

To measure the surface temperature of the panel, five k-type thermos couples were axially installed at the center of the PV panel. The arithmetic average of the temperature reading was considered as a surface temperature. To calculate the equivalent thermal–electrical value of the system, the following equation was employed:

$$\Xi = \frac{E_{el.} - E_{pump}}{0.38}, \tag{4}$$

where,  $E_{el.}$  is the electricity produced with the PV panel and  $E_{pump}$  is the power consumed by the pump for circulating the nanofluids, which is supplied with the PV panel. In the present study, the equivalent thermal–electrical value was calculated at the peak time (1:30 pm to 3:30 pm). To calculate the uncertainty analysis, Kline–McClintock equation was utilized [44]. Table 2 shows the uncertainty values of the instruments used in the present research.

**Table 2.** The calculated uncertainty values of the parameters and instruments used in the present research.

Parameter	Instrument	Manufacturer	Accuracy/Uncertainty
Solar irradiance		Omni	±1% of reading value
Temperature of PV panel	k-type thermocouple	Omega	0.5 °C
Temperature of HTF	RTD	Omega	0.5 °C
Fluid flow	Ultrasonic flow meter	Flownetix	±1% of reading value
Voltage and current	Digital multi-meter	Omega	±1% of reading value
<b>Parameters</b>			
Electrical power	-	-	±1.5%
Thermal power	-	-	±2.1% including heat loss
Equivalent thermal–electrical power	-	-	±1.5%

### 3. Results

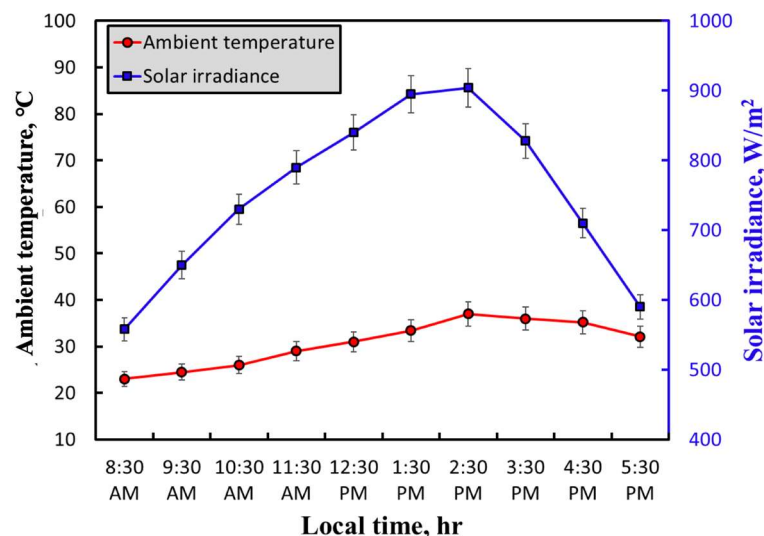
#### 3.1. Solar Irradiance and Ambient Temperature

Figure 4 shows the variation of the solar irradiance and the ambient temperature with local time measured on 15<sup>th</sup> August 2018. As can be seen, the ambient temperature gradually increased reaching the maximum of 35 °C at 2:30 pm and then slightly decreased. However, for solar irradiance, the story is different. The solar irradiance was minimum at 8:30 am (550 W/m<sup>2</sup>) and increased to 895 and 910 W/m<sup>2</sup> at 12:30 pm and 1:30 pm. Therefore, it is expected that the largest thermal production can be achieved at midday, however, due to the increase in the surface temperature of the solar panel, the electricity production might be affected as the resistance of the panel increases with an increase in the temperature of the panel. Hence, the performance of the cooling system must be regulated such that the surface temperature of PV be minimized from 1:30 pm to 3:30 pm to compensate for the increase in the solar irradiance. Also, heat loss to environment is another technical challenge, which can occur at high surface temperature. This can also be suppressed using an efficient cooling mechanism. Hence, the presence of the PCM plays a major role in absorbing the thermal energy from PV panel, particularly at midday.

#### 3.2. Surface Temperature of the PV Panel

Figure 5A represents the dependence of the surface temperature of the PV panel on the local time for water, WEG 50, and nano-suspensions at 0.1wt% to 0.3wt%. As can be seen, with time spanning from 8:30 am to 2:30 pm, the surface temperature of the PV panel increased following a non-linear

trend represented in Figure 5. For example, for the panel cooling with water at 8:30 am, the average surface temperature of the PV panel was  $\sim 32$  °C reaching 46 °C at 2:30 pm. However, for the same local times, the surface temperature of the PV panel was 31 °C and 42 °C for WEG, 50 °C, 29 °C, and 41 °C for 0.1wt%, and 26 °C and 36 °C for 0.3wt%, respectively. This can be attributed to the improvement in the thermo–physical characteristics of the working fluid. Water was also used as a reference case to compare the results with the ones already presented in the literature. An agreement of  $\pm 4\%$  is seen with the results published in the literature [30]. As can be seen, the presence of PCM and MWCNTs in the system further improved the thermal performance of the PV/T-PCM system. By adding MWCNTs to paraffin, the thermal conductivity of the PCM was improved by 19%, which in turn intensified the heat transfer rate between the backside of the PV panel and the cooling pipes passing through the PCM container. Also, due to the sensible thermal storage capability of MWCNT–paraffin PCM, the heat loss from the PV panel was absorbed by the PCM and transported to the coolant. The presence of MWCNTs in WEG 50 improved the thermal conductivity, Brownian motion and also the thermo-phoresis effect, which can be another reason for improving the thermal performance of the system. It is worth saying that the surface temperature data followed a polynomial trend, which is in good accordance with the results published in the literature. This trend was also in accordance with the experimental data collected with the pyrano-meter. Notably, nanofluids can considerably change the thermal performance of the system. This is because a chain of mechanisms is added to the system including Brownian motion, thermophoresis effect, Benard–Maragoni effect and also the inherent increase in the thermal conductivity of the nanofluid. These mechanisms always result in the promotion of the thermal performance of the system [45–50] in comparison with the conventional single and two-phase systems as shown in our previous study [51,52].



**Figure 4.** Dependence of the ambient temperature and solar irradiance on local time.

Figure 5B shows the current-voltage (I–V) curve obtained for the PV cooling with various nanofluids. As can be seen, the peak of power production (122 W) is seen at 22.5 V for nanofluid at 0.3wt%. However, it is expected that the pumping power associated with the pressure drop of the system is also the highest at 0.3wt%. Hence, despite higher power production, still a portion of the electricity is consumed for pumping the nanofluids into the system, which affects the thermal–electricity equivalent power of the system. As can also be seen, with an increase in the mass concentration of the nanofluid, the cooling performance is improved, which in turn promotes the power production of the PV system.

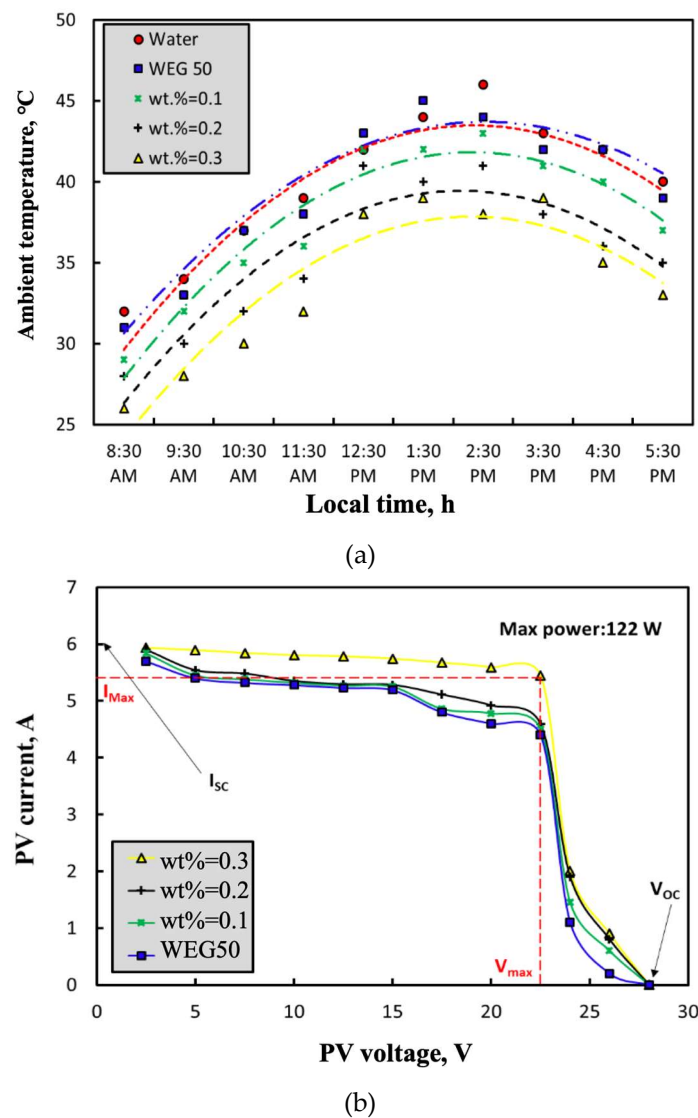


**Figure 5.** (a) Dependence of the surface temperature of the PV panel on local time for various mass concentration of the nanofluids, (b) Current-Voltage (I–V) curve obtained for the PV cooling with various nanofluids.

### 3.3. Flow Rate of Cooling Loop

Figure 6 shows the variation of the surface temperature of the PV panel with the flow rate of the cooling loop for WEG 50 (base fluid) and nano-suspensions at various mass fractions of MWCNTs. As can be seen, with an increase in the flow rate of the coolant, the surface temperature of the PV panel decreased. For example, at a flow rate of 0.1 L/min, the surface temperature of the PV panel cooled with WEG 50 was 32 °C, reaching 27 °C at 1.0 L/min. This was because with an increase in the fluid flow, the velocity of the HTF increased, which in turn improved the convective heat transfer within the pipes. The larger the convective heat transfer, the larger the heat transfer between the PCM and the pipes inside the PCM container. Interestingly, with an increase in the mass concentration of the MWCNTs, the performance of the system was intensified, which is in accordance with the results already discussed in Figure 4. For example, at a flow rate of 0.1 L/min, the surface temperature of the PV panel cooled with WEG 50 was 32 °C, however, the surface temperature of the PV panel for the same given flow rate was 29 °C, 28 °C, and 26 °C for nano-suspensions at 0.1wt%, 0.2wt%, and 0.3wt%, respectively. This was attributed to the improvement in the thermal performance of the coolant due to the enhancement in the thermal conductivity of the base fluid.

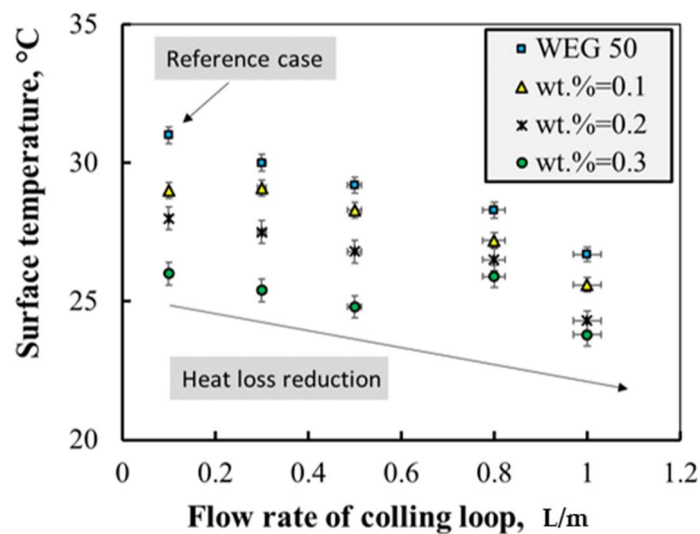


**Figure 6.** Dependence of the surface temperature of the PV panel on flow rate of cooling loop for various mass concentration of the nanofluids.

### 3.4. Electricity Production

Figure 7 presents the dependence of the power production by the PV panel on the local time for different coolants used in the cooling system. Since the electricity production of a PV panel is strongly influenced by the temperature of the panel, it is crucial to maintain a uniform cooling rate to the PV panel to reduce the surface temperature of the panel below the maximum threshold allowable for the PV panel. As can be seen from the figure, the electrical power production of the PV panel was promoted with an increase in the mass fraction of MWCNTs. For example, at 2:30 pm which is the peak of the production, for the panel cooled with WEG 50, the power production reached  $102 \text{ W/m}^2$ , while for the PV panel cooled with nanofluids at 0.1wt%, 0.2wt%, and 0.3wt%, the power production reached  $110 \text{ W/m}^2$ ,  $116 \text{ W/m}^2$ , and  $122 \text{ W/m}^2$ , respectively. By integrating the area captured by the power production–local time figure, it can be understood that ~45% of the total electricity production occurred at midday from 12:30 pm to 3:30 pm and the production of the electricity was larger for the PV panels cooled with nanofluids (2% to 5.6% larger than that of recorded for WEG 50). Interestingly, from 8:30 am to 12:30 pm, about 35% of the total electricity was produced with the PV panel and the rest was produced after 3:30 pm (~20%). This reveals the importance of the cooling loop in a PVT system. It is worth saying that the presence of the MWCNT-PCM not only fortifies the thermal energy absorption from the PV panel, but also improves the thermal performance of the system by transporting the thermal energy to the cooling pipes. Notably, a case study was also conducted without the PCM within the PV panel and a reduction of 15% in thermal performance was observed. This is because a portion of thermal energy was purged to the environment as a heat loss. Likewise, the presence of MWCNT-PCM and MWCNT–WEG 50 caused a more uniform heat transfer within the PV panel compared to WEG 50, which was due to the enhancement in the thermal diffusivity and thermal conductivity of the working fluid.

### 3.5. Thermal Power Production

Figure 8 shows the variation of the thermal power production of the PV panel with the local time for the PV panel cooling with various HTFs including WEG 50 and nano-suspensions at 0.1wt%, 0.2wt%, and 0.3wt%, respectively. As can be seen, the thermal power production of the PV increased with time spanning from 8:30 am to 2:30 pm and then decreased as the solar irradiance was suppressed in the afternoon. Similar to the electrical power production, the thermal power was intensified by increasing the mass fraction of the nanofluid such that the largest thermal power production was  $260 \text{ W/m}^2$  observed at 2:30 pm for MWCNT–WEG 50 nanofluid at 0.3wt%. For the same local time, the

power production was 202 W/m<sup>2</sup>, 195 W/m<sup>2</sup>, and 115 W/m<sup>2</sup> for nanofluids at 0.2wt% and 0.1wt% and WEG 50, respectively. Notably, the power production–local time trend follows the trend identified for solar irradiance. It is worth saying that the change in the rate of the power production for PV cooling with WEG 50 was relatively smaller than that of observed for nanofluids. To further evaluate the effect of PCM on the thermal performance of PV, a case study was conducted with water and no PCM. As can be seen, for this case, the absence of PCM material resulted in the decrease in thermal energy production of the system. Also, the absence of MWCNTs within the system further decreased the cooling performance of the PV system resulting in a decrease in thermal energy production of the PV panel.

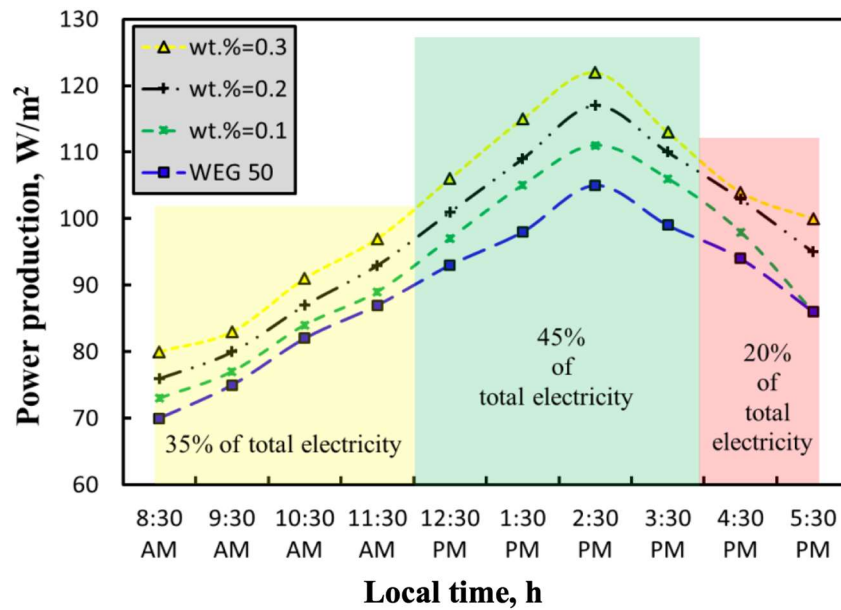


Figure 7. Dependence of the electrical power production of the PV panel on local time for various mass concentration of the nanofluids.

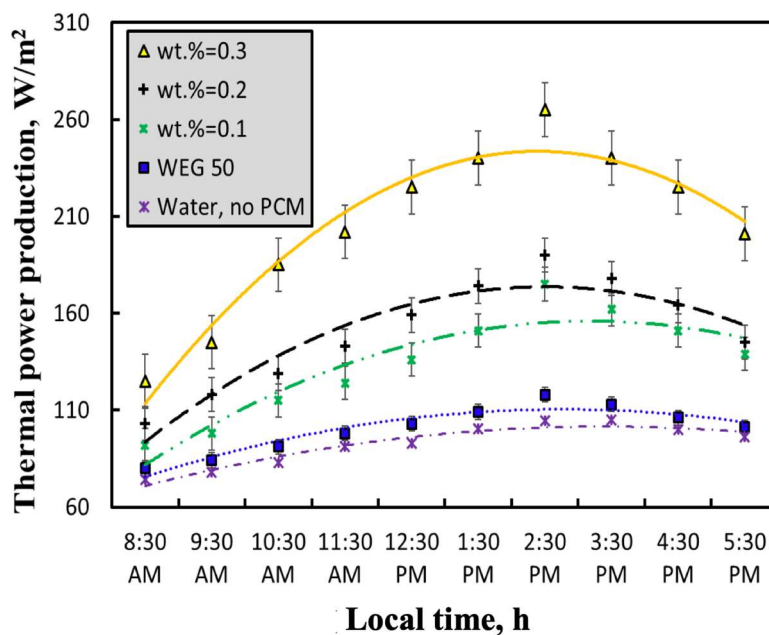
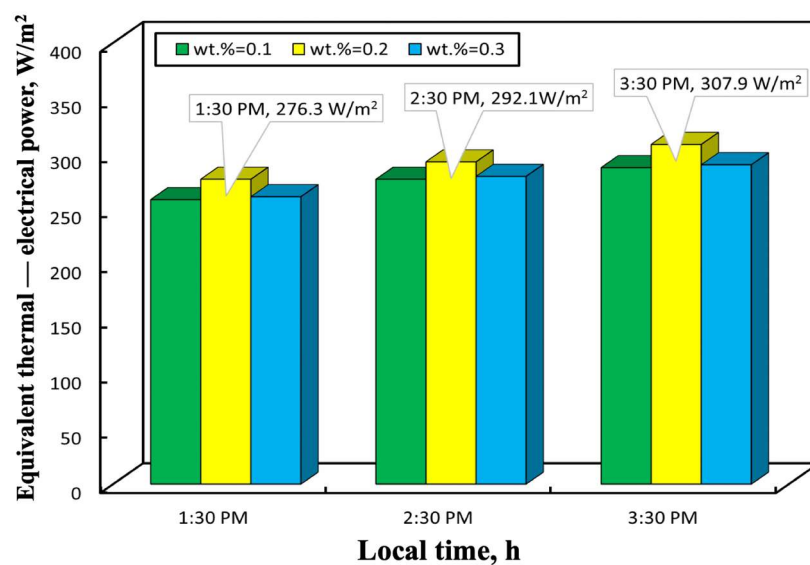


Figure 8. Dependence of the thermal power production of the PV panel on local time for various mass concentration of nanofluids.

### 3.6. Electrical–Thermal Equivalent Power

To better analyze the performance of the PV/T–PCM system, the electrical power must also be converted to the thermal energy to provide a back to back comparison with other power production systems. Hence, the conversion factor of 0.38 was employed as suggested in the literature. Figure 9 shows the variation of the measured equivalent thermal–electrical value of the system with the local time for nanofluids at 0.1wt% to 0.3wt%. As can be seen, the largest equivalent thermal–electrical value was observed at 3:30 pm and for nanofluid at 0.2wt%. This is because, with an increase in the mass fraction of the nanofluid, the viscosity and also the pumping power required for circulation of the nanofluid increased, which in turn decreased the equivalent electrical–thermal value of the system. Therefore, it can be concluded that the plausible mass fraction of MWCNT for dispersion in WEG 50 for cooling a PV panel is 0.2. The largest equivalent electrical–thermal power was 307.9 W/m<sup>2</sup> which is competitive with the results reported in the literature.



**Figure 9.** Variation of the equivalent electrical–thermal power production with mass concentration of the nanofluids during the peak of power production from 1:30 pm to 3:30 pm.

## 4. Conclusions

An experimental investigation was conducted to evaluate the electrical and thermal power production of a PV/T system equipped with a cooling jacket filled with MWCNT–paraffin as the PCM. Results showed that the presence of MWCNT–WEG 50 nanofluid improved the thermal performance of the system, electrical (~20% enhancement) and thermal production of the system (~130%), which was attributed to the reduction of the surface temperature of the PV panel, absorption of the thermal energy from PV panel with the PCM and also the improvement in the thermal conductivity of the PCM and the heat transfer fluid. The equivalent thermal–electrical value of the system during the peak time reached 276.3 W/m<sup>2</sup> to 307.9 W/m<sup>2</sup> showing the plausible application of the system for the co-production of thermal and electrical power with nanofluids. Also, the system was self-sustained and supplied the required energy for circulating the HTF within the system. However, further study on the heat transfer coefficient between the PCM and PV panel, heat transfer coefficient between the PCM and working fluid, and also a fundamental study on the role of nanoparticles on the thermal properties of PCMs is highly recommended to be conducted.

**Author Contributions:** Conceptualization, M.M.S.; methodology, M.M.S., M.R.S., M.G., M.A.; formal analysis, M.M.S., M.R.S., M.G., I.T., Z.T., T.A.A.; investigation, M.M.S., M.G., M.A.; writing—original draft preparation, M.M.S., Z.T., I.T., T.A.A., M.J., A.S.L., M.G.; writing—review and editing, M.M.S., M.R.S., A.S.L., M.A., I.T., T.A.A., Z.T.; supervision, M.M.S., M.A., A.S.L.

**Funding:** This research is partially supported by the Key Laboratory of Fluid Power and Intelligent Electro-Hydraulic Control (Fuzhou University), Fundamental Research Fund for Central Universities (201941008), and Taishan Scholar (tsqn201812025).

**Acknowledgments:** The authors would like to acknowledge the Rayan Sanat Company for sharing the PV facilities. The authors would also like to thank O. S. Javid for helping the authors collecting the solar data. Last but not least, the authors extend their appreciation to the Deanship of Scientific Research at Majmaah University for funding this work under project number No. (RGP-2019-17).

**Conflicts of Interest:** The authors declare no conflict of interest.

## References

1. Kampa, M.; Castanas, E. Human health effects of air pollution. *Environ. Pollut.* **2008**, *151*, 362–367. [[CrossRef](#)] [[PubMed](#)]
2. Solangi, K.; Islam, M.; Saidur, R.; Rahim, N.; Fayaz, H. A review on global solar energy policy. *Renew. Sustain. Energy Rev.* **2011**, *15*, 2149–2163. [[CrossRef](#)]
3. Kalogirou, S. The potential of solar industrial process heat applications. *Appl. Energy* **2003**, *76*, 337–361. [[CrossRef](#)]
4. Valencia, G.; Benavides, A.; Cárdenas, Y. Economic and environmental multiobjective optimization of a wind–solar–fuel cell hybrid energy system in the colombian caribbean region. *Energies* **2019**, *12*, 2119. [[CrossRef](#)]
5. Szokolay, S.V. *Solar Energy and Building*; Halsted Press Division, Wiley: New York, NY, USA, 1975.
6. Liu, X.; Wang, Y. Reconfiguration method to extract more power from partially shaded photovoltaic arrays with series-parallel topology. *Energies* **2019**, *12*, 1439. [[CrossRef](#)]
7. Kharseh, M.; Wallbaum, H. How adding a battery to a grid-connected photovoltaic system can increase its economic performance: A comparison of different scenarios. *Energies* **2019**, *12*, 30. [[CrossRef](#)]
8. Chandel, S.; Naik, M.N.; Chandel, R. Review of solar photovoltaic water pumping system technology for irrigation and community drinking water supplies. *Renew. Sustain. Energy Rev.* **2015**, *49*, 1084–1099. [[CrossRef](#)]
9. Chow, T.; Hand, J.; Strachan, P. Building-integrated photovoltaic and thermal applications in a subtropical hotel building. *Appl. Therm. Eng.* **2003**, *23*, 2035–2049. [[CrossRef](#)]
10. Prakash, J. Transient analysis of a photovoltaic-thermal solar collector for co-generation of electricity and hot air/water. *Energy Convers. Manag.* **1994**, *35*, 967–972. [[CrossRef](#)]
11. Alshayeb, M.; Chang, J. Variations of pv panel performance installed over a vegetated roof and a conventional black roof. *Energies* **2018**, *11*, 1110. [[CrossRef](#)]
12. Mani, M.; Pillai, R. Impact of dust on solar photovoltaic (pv) performance: Research status, challenges and recommendations. *Renew. Sustain. Energy Rev.* **2010**, *14*, 3124–3131. [[CrossRef](#)]
13. Al Dakheel, J.; Tabet Aoul, K. Building applications, opportunities and challenges of active shading systems: A state-of-the-art review. *Energies* **2017**, *10*, 1672. [[CrossRef](#)]
14. Erdil, E.; Ilkan, M.; Egelioglu, F. An experimental study on energy generation with a photovoltaic (pv)–solar thermal hybrid system. *Energy* **2008**, *33*, 1241–1245. [[CrossRef](#)]
15. Odeh, S. Thermal performance of dwellings with rooftop pv panels and pv/thermal collectors. *Energies* **2018**, *11*, 1879. [[CrossRef](#)]
16. Abdollahi-Moghaddam, M.; Rejvani, M.; Alamdari, P. Determining optimal formulations and operating conditions for al<sub>2</sub>o<sub>3</sub>/water nanofluid flowing through a microchannel heat sink for cooling system purposes using statistical and optimization tools. *Therm. Sci. Eng. Prog.* **2018**, *8*, 517–524. [[CrossRef](#)]
17. Safaei, M.; Ahmadi, G.; Goodarzi, M.; Safdari Shadloo, M.; Goshayeshi, H.; Dahari, M. Heat transfer and pressure drop in fully developed turbulent flows of graphene nanoplatelets–silver/water nanofluids. *Fluids* **2016**, *1*, 20. [[CrossRef](#)]
18. Moghaddam, M.A.; Motahari, K. Experimental investigation, sensitivity analysis and modeling of rheological behavior of mwcnt-cuo (30–70)/sae40 hybrid nano-lubricant. *Appl. Therm. Eng.* **2017**, *123*, 1419–1433. [[CrossRef](#)]
19. Farshad, S.A.; Sheikholeslami, M. Nanofluid flow inside a solar collector utilizing twisted tape considering exergy and entropy analysis. *Renew. Energy* **2019**, *141*, 246–258. [[CrossRef](#)]



20. Yazdanifard, F.; Ameri, M.; Ebrahimnia-Bajestan, E. Performance of nanofluid-based photovoltaic/thermal systems: A review. *Renew. Sustain. Energy Rev.* **2017**, *76*, 323–352. [[CrossRef](#)]
21. Sahota, L.; Tiwari, G. Analytical characteristic equation of nanofluid loaded active double slope solar still coupled with helically coiled heat exchanger. *Energy Convers. Manag.* **2017**, *135*, 308–326. [[CrossRef](#)]
22. Al-Waeli, A.H.; Sopian, K.; Kazem, H.A.; Chaichan, M.T. Photovoltaic solar thermal (pv/t) collectors past, present and future: A. *Int. J. Appl. Eng. Res.* **2016**, *11*, 10757–10765.
23. Hasan, A.; Alnoman, H.; Shah, A. Energy efficiency enhancement of photovoltaics by phase change materials through thermal energy recovery. *Energies* **2016**, *9*, 782. [[CrossRef](#)]
24. Safaei, M.R.; Goshayeshi, H.R.; Chaer, I. Solar still efficiency enhancement by using graphene oxide/paraffin nano-pcm. *Energies* **2019**, *12*, 2002. [[CrossRef](#)]
25. Kazanci, O.B.; Skrupskelis, M.; Sevela, P.; Pavlov, G.K.; Olesen, B.W. Sustainable heating, cooling and ventilation of a plus-energy house via photovoltaic/thermal panels. *Energy Build.* **2014**, *83*, 122–129. [[CrossRef](#)]
26. Al-Waeli, A.H.; Sopian, K.; Chaichan, M.T.; Kazem, H.A.; Ibrahim, A.; Mat, S.; Ruslan, M.H. Evaluation of the nanofluid and nano-pcm based photovoltaic thermal (pvt) system: An experimental study. *Energy Convers. Manag.* **2017**, *151*, 693–708. [[CrossRef](#)]
27. Sardarabadi, M.; Passandideh-Fard, M.; Maghrebi, M.-J.; Ghazikhani, M. Experimental study of using both zno/water nanofluid and phase change material (pcm) in photovoltaic thermal systems. *Sol. Energy Mater. Sol. Cells* **2017**, *161*, 62–69. [[CrossRef](#)]
28. Al-Waeli, A.H.; Kazem, H.A.; Chaichan, M.T.; Sopian, K. Experimental investigation of using nano-pcm/nanofluid on a photovoltaic thermal system (pvt): Technical and economic study. *Therm. Sci. Eng. Prog.* **2019**, *11*, 213–230. [[CrossRef](#)]
29. Hosseinzadeh, M.; Sardarabadi, M.; Passandideh-Fard, M. Energy and exergy analysis of nanofluid based photovoltaic thermal system integrated with phase change material. *Energy* **2018**, *147*, 636–647. [[CrossRef](#)]
30. Al-Waeli, A.H.; Chaichan, M.T.; Sopian, K.; Kazem, H.A.; Mahood, H.B.; Khadom, A.A. Modeling and experimental validation of a pvt system using nanofluid coolant and nano-pcm. *Sol. Energy* **2019**, *177*, 178–191. [[CrossRef](#)]
31. Hasan, H.A.; Sopian, K.; Jaaz, A.H.; Al-Shamani, A.N. Experimental investigation of jet array nanofluids impingement in photovoltaic/thermal collector. *Sol. Energy* **2017**, *144*, 321–334. [[CrossRef](#)]
32. Al-Shamani, A.N.; Sopian, K.; Mat, S.; Hasan, H.A.; Abed, A.M.; Ruslan, M.H. Experimental studies of rectangular tube absorber photovoltaic thermal collector with various types of nanofluids under the tropical climate conditions. *Energy Convers. Manag.* **2016**, *124*, 528–542. [[CrossRef](#)]
33. Hussain, M.I.; Kim, J.-H.; Kim, J.-T. Nanofluid-powered dual-fluid photovoltaic/thermal (pv/t) system: Comparative numerical study. *Energies* **2019**, *12*, 775. [[CrossRef](#)]
34. Al-Waeli, A.H.; Chaichan, M.T.; Kazem, H.A.; Sopian, K. Comparative study to use nano-(al<sub>2</sub>o<sub>3</sub>, cuo, and sic) with water to enhance photovoltaic thermal pv/t collectors. *Energy Convers. Manag.* **2017**, *148*, 963–973. [[CrossRef](#)]
35. Al-Waeli, A.H.; Chaichan, M.T.; Kazem, H.A.; Sopian, K.; Safaei, J. Numerical study on the effect of operating nanofluids of photovoltaic thermal system (pv/t) on the convective heat transfer. *Case Stud. Therm. Eng.* **2018**, *12*, 405–413. [[CrossRef](#)]
36. Aberoumand, S.; Ghamari, S.; Shabani, B. Energy and exergy analysis of a photovoltaic thermal (pv/t) system using nanofluids: An experimental study. *Sol. Energy* **2018**, *165*, 167–177. [[CrossRef](#)]
37. Lari, M.O.; Sahin, A.Z. Effect of retrofitting a silver/water nanofluid-based photovoltaic/thermal (pv/t) system with a pcm-thermal battery for residential applications. *Renew. Energy* **2018**, *122*, 98–107. [[CrossRef](#)]
38. Al-Waeli, A.H.; Sopian, K.; Kazem, H.A.; Yousif, J.H.; Chaichan, M.T.; Ibrahim, A.; Mat, S.; Ruslan, M.H. Comparison of prediction methods of pv/t nanofluid and nano-pcm system using a measured dataset and artificial neural network. *Sol. Energy* **2018**, *162*, 378–396. [[CrossRef](#)]
39. Abdallah, S.R.; Saidani-Scott, H.; Abdellatif, O.E. Performance analysis for hybrid pv/t system using low concentration mwcnt (water-based) nanofluid. *Sol. Energy* **2019**, *181*, 108–115. [[CrossRef](#)]
40. Al-Waeli, A.H.A.; Sopian, K.; Yousif, J.H.; Kazem, H.A.; Boland, J.; Chaichan, M.T. Artificial neural network modeling and analysis of photovoltaic/thermal system based on the experimental study. *Energy Convers. Manag.* **2019**, *186*, 368–379. [[CrossRef](#)]

41. Salem, M.R.; Elsayed, M.M.; Abd-Elaziz, A.A.; Elshazly, K.M. Performance enhancement of the photovoltaic cells using  $Al_2O_3/PCM$  mixture and/or water cooling-techniques. *Renew. Energy* **2019**, *138*, 876–890. [[CrossRef](#)]
42. Fayaz, H.; Rahim, N.A.; Hasanuzzaman, M.; Nasrin, R.; Rivai, A. Numerical and experimental investigation of the effect of operating conditions on performance of pvt and pvt-pcm. *Renew. Energy* **2019**, *143*, 827–841. [[CrossRef](#)]
43. Fayaz, H.; Rahim, N.A.; Hasanuzzaman, M.; Rivai, A.; Nasrin, R. Numerical and outdoor real time experimental investigation of performance of pcm based pvt system. *Sol. Energy* **2019**, *179*, 135–150. [[CrossRef](#)]
44. Kline, S.J. Describing uncertainty in single sample experiments. *Mech. Eng.* **1953**, *75*, 3–8.
45. Arya, A.; Sarafraz, M.; Shahmiri, S.; Madani, S.; Nikkhah, V.; Nakhjavani, S. Thermal performance analysis of a flat heat pipe working with carbon nanotube-water nanofluid for cooling of a high heat flux heater. *Heat Mass Transf.* **2018**, *54*, 985–997. [[CrossRef](#)]
46. Salari, E.; Peyghambarzadeh, M.; Sarafraz, M.M.; Hormozi, F. Boiling heat transfer of alumina nano-fluids: Role of nanoparticle deposition on the boiling heat transfer coefficient. *Period. Polytech. Chem. Eng.* **2016**, *60*, 252–258. [[CrossRef](#)]
47. Salari, E.; Peyghambarzadeh, S.; Sarafraz, M.; Hormozi, F.; Nikkhah, V. Thermal behavior of aqueous iron oxide nano-fluid as a coolant on a flat disc heater under the pool boiling condition. *Heat Mass Transf.* **2017**, *53*, 265–275. [[CrossRef](#)]
48. Sarafraz, M.; Arjomandi, M. Demonstration of plausible application of gallium nano-suspension in microchannel solar thermal receiver: Experimental assessment of thermo-hydraulic performance of microchannel. *Int. Commun. Heat Mass Transf.* **2018**, *94*, 39–46. [[CrossRef](#)]
49. Sarafraz, M.; Arya, A.; Nikkhah, V.; Hormozi, F. Thermal performance and viscosity of biologically produced silver/coconut oil nanofluids. *Chem. Biochem. Eng. Q.* **2017**, *30*, 489–500. [[CrossRef](#)]
50. Sarafraz, M.; Arjomandi, M. Thermal performance analysis of a microchannel heat sink cooling with copper oxide-indium (CuO/In) nano-suspensions at high-temperatures. *Appl. Therm. Eng.* **2018**, *137*, 700–709. [[CrossRef](#)]
51. Sarafraz, M. Experimental investigation on pool boiling heat transfer to formic acid, propanol and 2-butanol pure liquids under the atmospheric pressure. *J. Appl. Fluid Mech.* **2013**, *6*, 73–79.
52. Sarafraz, S.; Peyghambarzadeh, M.; Vaeli, N. Subcooled flow boiling heat transfer of ethanol aqueous solutions in vertical annulus space. *Chem. Ind. Chem. Eng. Q. CICEQ* **2012**, *18*, 315–327. [[CrossRef](#)]



© 2019 by the authors. Licensee MDPI, Basel, Switzerland. This article is an open access article distributed under the terms and conditions of the Creative Commons Attribution (CC BY) license (<http://creativecommons.org/licenses/by/4.0/>).